Sound propagation in liquid helium near the λ point. II. Ultrasonic attenuation

Richard A. Ferrell and Behzad Mirhashem
Center for Theoretical Physics of the Department of Physics and Astronomy, University of Maryland, College Park, Maryland 20742

Jayanta K. Bhattacharjee
Department of Physics, Indian Institute of Technology, Kanpur 208016, U.P., India
(Received 15 October 1986)

We present an improved theory of critical ultrasonic attenuation above the λ point that is in good agreement with the experimental data. Static interactions are taken into account by means of a simple modification of the single-loop specific-heat integral. Dynamic interactions, important in the crossover regime at low frequencies, produce a frequency-dependent change in the kinetic coefficient, without otherwise changing the scaling function.

I. INTRODUCTION

The general physical mechanism for the critical ultrasonic attenuation in fluids has been identified[1] as the temperature swings associated with the adiabatic compressions and rarefactions. Generalizing the Herzfeld-Rice[2] theory of ultrasonic attenuation in gases, we have been able to characterize the critical attenuation in fluids entirely in terms of the dynamic scaling properties of the frequency-dependent specific heat. The good agreement[3] in the magnitude of the critical attenuation at the λ point of liquid ^{4}He and the excellent agreement[4] at the consolute point of the binary liquid 3-methylpentane-nitroethane give us confidence that we have correctly identified the mechanism for the critical attenuation.

In this paper we return to the λ-point attenuation, making use of our detailed thermodynamic study[5] of the propagation of sound near the λ point. Benefiting also from our work on the binary liquid,[6] we are able to take into account, to some extent, the interaction of the order-parameter fluctuations. The resulting improvement in the comparison of our theory with experiment is presented in Sec. II.

Our second goal is to extend our theory down to lower frequencies. This takes us out of the van Hove region, where the kinetic coefficient is a constant, and into the more complicated precritical and crossover regimes. By means of a perturbation approach, the full theoretical details of which we intend to present in a subsequent paper,[7] we have found that, to a good approximation, the shape of the scaling function remains unchanged. For fitting the temperature dependence of the attenuation as the λ point is approached, it is only necessary to rescale the kinetic coefficient by a factor which depends upon the particular frequency at which the run of measurements is made. Section III illustrates, purely empirically, how this procedure works in the crossover region. The values of the kinetic coefficient that are required in order to fit runs at seven different frequencies are exhibited in Fig. 7 below as a function of the frequency, the lowest frequency being 0.6 MHz. Section IV is a general discussion and summary.

II. FREQUENCY-DEPENDENT SPECIFIC HEAT

From Ref. 3, and from Eq. (13) of Ref. 5, it follows that the critical attenuation in one wavelength is

$$\alpha\lambda = -\frac{K_0}{2\pi} C_\lambda \mathrm{Im} C_P^{-1} , \tag{2.1}$$

where K_0 and C_λ are purely thermodynamic quantities. We found[5] $K_0 \simeq 9\times 10^{-3}$, while C_λ is the specific heat along the λ line. C_λ is equal to the thermodynamic constant-pressure specific heat C_p at the temperature of maximum density, $T - T_\lambda = 6$ mK above the λ point for saturated vapor pressure. This paper is restricted to saturated vapor pressure and to $T > T_\lambda$. In order to apply Eq. (2.1) we need for C_P an appropriate complex function of the frequency ω. This is rather complicated below the λ point,[8] but is relatively simple above the λ point, where we can assume that the order-parameter fluctuations are damped and nonpropagating. In the van Hove region, at sufficiently large reciprocal correlation length κ, the kinetic coefficient D_ψ takes on its constant background value B_ψ, and the relaxation rate of an order-parameter fluctuation of wave number k is

$$\tfrac{1}{2}\gamma(k,\kappa) = B_\psi g^{-1}(k,\kappa) . \tag{2.2}$$

For the critical correlation function we use the Ornstein-Zernike approximation

$$g(k,\kappa) = \frac{1}{k^2+\kappa^2} . \tag{2.3}$$

The $k=0$ limit of Eq. (2.2) provides the characteristic temperature-dependent pair relaxation rate

$$\gamma(\kappa) \equiv \gamma(0,\kappa) = 2B_\psi \kappa^2 . \tag{2.4}$$

It is convenient to express the frequency in terms of

$$Z = \frac{-i\omega}{2B_\psi} , \tag{2.5}$$

and the scaled frequency $\Omega = \omega/\gamma$ in terms of

$$z = \frac{Z}{\kappa^2} = -i\frac{\omega}{\gamma} = -i\Omega . \tag{2.6}$$

The noninteracting single-loop expression for the frequency-dependent specific heat in $D=4-\epsilon$ dimensions is given by the dimensionless integral

$$I_D(\kappa,Z)=\frac{k_c^{\epsilon}}{C_D}\int d^D k\, g^2(k,\kappa)\frac{\gamma(k,\kappa)}{\gamma(k,\kappa)-i\omega}\ , \tag{2.7}$$

where C_D is the area of the unit sphere and k_c is a characteristic wave number. Substituting Eqs. (2.2), (2.3), and (2.5) in Eq. (2.7) yields

$$I_D(\kappa,Z)=k_c^{\epsilon}\int\frac{k^{D-1}dk}{(k^2+\kappa^2)(k^2+\kappa^2+Z)}\ . \tag{2.8}$$

The $\epsilon=0$ limit requires an upper cutoff q_D, for which we find

$$\begin{aligned} I_D(\kappa,Z)&=\ln\frac{q_D}{\kappa}-\tfrac{1}{2}(1+1/z)\ln(1+z)\\ &=I_4(\kappa,0)+\Delta I_4(z)\ . \end{aligned} \tag{2.9}$$

This simple formula is applicable when the two inequalities $\kappa\ll q_D$ and $|Z|^{1/2}\ll q_D$ are both satisfied. The evaluation of the integral for the general case is straightforward and yields a tractable but somewhat more complicated expression. The thermodynamic specific heat is represented by

$$I_4(\kappa,0)=\ln\frac{q_D}{\kappa}-\frac{1}{2}\ , \tag{2.10}$$

supplemented by an appropriate background term. The deviation from the thermodynamic specific heat is expressed by the scaling function

$$\Delta I_4(z)=\tfrac{1}{2}-\tfrac{1}{2}(1+1/z)\ln(1+z)\ , \tag{2.11}$$

as found in Eq. (12) of Ref. 3. For $|z|\gg 1$, Eq. (2.11) becomes

$$\Delta I_4=\tfrac{1}{2}\ln\frac{a_4}{z}-\frac{1}{2z}(\ln z+1)+O(z^{-2})\ , \tag{2.12a}$$

with $a_4=e$. For $|z|\ll 1$ we have

$$\Delta I_4=-\tfrac{1}{4}z+\tfrac{1}{12}z^2-\tfrac{1}{24}z^3+O(z^4)\ . \tag{2.12b}$$

In contrast to the thermodynamic function of Eq. (2.10), the frequency-dependent specific heat has the finite λ-point limit

$$\begin{aligned} I_4(0,Z)&=-\tfrac{1}{2}\ln\frac{Z}{q_D^2}\\ &=\tfrac{1}{2}\ln\frac{2B_{\psi}q_D^2}{\omega}+i\frac{\pi}{4}\ . \end{aligned} \tag{2.12c}$$

From Eq. (2.1), the attenuation is proportional to

$$-\mathrm{Im}C_P^{-1}\propto\frac{\mathrm{Im}I_4}{|I_4|^2}\ , \tag{2.13}$$

with the numerator varying more strongly than the denominator. Concentrating our attention on the numerator and normalizing it to its λ-point value gives the "attenuation function"

$$F_4(\Omega)=\frac{\mathrm{Im}I_4(\kappa,Z)}{\mathrm{Im}I_4(0,Z)}=\frac{2}{\pi}\tan^{-1}\Omega-\frac{1}{\pi\Omega}\ln(1+\Omega^2)\ , \tag{2.14}$$

equivalent to Eq. (13b) of Ref. 3. At low reduced frequencies, $\Omega\ll 1$,

$$\pi F_4=\Omega-\frac{\Omega^3}{6}+O(\Omega^5)\ . \tag{2.15}$$

The approach to the λ point for $\Omega\gg 1$ is governed by

$$\pi(1-F_4)=\frac{2}{\Omega}(1+\ln\Omega)+O(\Omega^{-2})\ , \tag{2.16}$$

as also follows directly from Eq. (2.12a).

In Ref. 6 we argue that we can improve upon the above $\epsilon=0$ treatment, which completely neglects the interaction of the fluctuations, by computing $I_D(\kappa,Z)$ for $D=3$ instead of for $D=4$, and then raising I_3 to the power that gives the correct critical specific-heat exponent. This procedure takes account of the interaction to first order in ϵ. In the present case of vanishing critical exponent, we pursue this approach and represent the frequency-dependent specific heat as

$$L_3(\kappa,Z)=\ln I_3(\kappa,Z)=L_3(\kappa,0)+\Delta L_3(z)\ , \tag{2.17}$$

with Eq. (2.8) evaluated as

$$I_3(\kappa,Z)=\frac{\pi k_c/2}{\kappa+(\kappa^2+Z)^{1/2}}\ . \tag{2.18}$$

The thermodynamic function (background to be added) is therefore

$$L_c(\kappa,0)=\ln\frac{\pi k_c}{4\kappa}\ , \tag{2.19}$$

while the new scaling function is

$$\Delta L_3(z)=\ln\frac{2}{1+(1+z)^{1/2}}\ . \tag{2.20}$$

For $|z|\gg 1$ this becomes

$$\Delta L_3\simeq\tfrac{1}{2}\ln\frac{a_3}{z}-z^{1/2}+O(z^{-3/2})\ , \tag{2.21a}$$

with $a_3=4$. For $|z|\ll 1$ we have

$$\Delta L_3=-\tfrac{1}{4}z+\tfrac{3}{32}z^2-\tfrac{5}{96}z^3+O(z^4)\ . \tag{2.21b}$$

At the λ point, Eq. (2.18) becomes

$$L_3(0,Z)=\tfrac{1}{2}\ln\frac{\pi^2 B_{\psi}k_c^2}{2\omega}+i\frac{\pi}{4}\ , \tag{2.21c}$$

with the same imaginary part as in the $\epsilon=0$ expression of Eq. (2.12c). The new "attenuation function" is

$$F_3(\Omega)=\frac{4}{\pi}\tan^{-1}\frac{[(1+\Omega^2)^{1/2}-1]^{1/2}}{\sqrt{2}+[(1+\Omega)^{1/2}+1]^{1/2}}\ , \tag{2.22}$$

whose low- and high-frequency behavior is given by

$$\pi F_3=\Omega-\tfrac{5}{24}\Omega^3+O(\Omega^5) \tag{2.23}$$

and

$$\pi(1-F_3)=2\left[\frac{2}{\Omega}\right]^{1/2}+O(\Omega^{-3/2}) . \quad (2.24)$$

These results also follow directly from Eqs. (2.21a) and (2.21b).

The dashed and solid curves of Fig. 1 show F_4 and F_3, respectively, plotted versus $\log_{10}\Omega$. The slightly more negative coefficient of the second term in Eq. (2.23), compared to the corresponding term in Eq. (2.15), causes F_3 to drop below F_4 with increasing Ω. The comparison of Eq. (2.24) with Eq. (2.16) indicates the much slower approach of F_3 to its λ-point limit, as is evident in the solid curve of Fig. 1. The maximum difference between the two curves in the high-frequency range is 7%.

The slower λ-point approach of the $D=3$ function is also exhibited by the spectral function. This is the imaginary part of the specific heat, analytically continued to the cut along the negative z axis, $z=-s<-1$. As discussed in Sec. VI of Ref. 6, the spectral function expresses the effective distribution of relaxing modes. The threshold at the minimum rate $\gamma(\kappa)=\gamma(0,\kappa)$ [Eq. (2.4)] is described by the step function

$$\Theta(s-1)=\begin{cases}1, & s>1\\ 0, & s<1\end{cases} . \quad (2.25)$$

For $D=4$, analytic continuation of Eq. (2.11) to the lower edge of the cut yields

$$f_4(s)=\frac{2}{\pi}\mathrm{Im}\Delta I_4(e^{-i\pi}s)$$
$$=(1-1/s)\Theta(s-1) . \quad (2.26)$$

The corresponding evaluation of Eq. (2.20) at the cut gives

$$f_3(s)=\frac{2}{\pi}\tan^{-1}\sqrt{s-1}\,\Theta(s-1) . \quad (2.27)$$

At large relative relaxation rates, $s\gg 1$, this becomes

$$f(s)\simeq 1-\frac{2}{\pi\sqrt{s}} , \quad (2.28)$$

corresponding to an effective deficiency of modes in this region, as seen by comparing the solid curve ($D=3$) with the dashed curve ($D=4$) in Fig. 2.

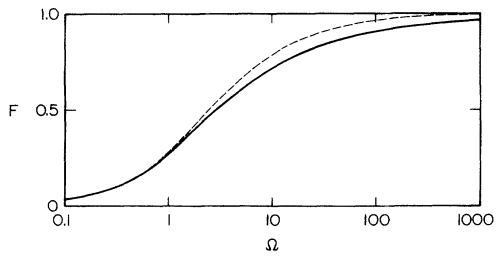

FIG. 1. Four-dimensional (dashed curve) and three-dimensional (solid curve) attenuation functions vs scaled frequency Ω.

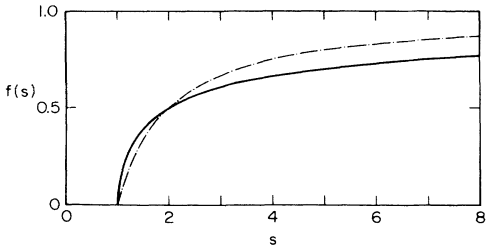

FIG. 2. Distribution of relaxation rates according to the four-dimensional (dot-dashed curve) and three-dimensional (solid curve) spectral functions vs scaled relaxation rate s.

The high-frequency approximation of Eq. (2.24) would predict a 50% drop in F_3 below its λ-point value of 1 at $\Omega=32/\pi^2\simeq 3.2$. To reach the actual halfway point we have to go down to the somewhat smaller value of $\Omega_{1/2}=2.8$, as exhibited by the solid curve of Fig. 1. Nevertheless, in the plot of F_3 versus $\Omega^{-1/2}$ in Fig. 3, a straight line gives an excellent fit in the entire region $\Omega_{1/2}\leq\Omega<\infty$. This property of F_3 is associated with the absence of any z^{-1} term in Eq. (2.21a). It is gratifying that the measurements of Roe, Mayer, and Ikushima[9] at 35 MHz clearly exhibit this linear dependence on $\Omega^{-1/2}$. The excellent agreement exhibited in Fig. 3 between the theoretical curve [F_3 of Eq. (2.22)] and the data of Roe *et al.*[9] confirms our expectation of the superiority of the $D=3$ version of the theory over our earlier $D=4$ version. We therefore employ only the $D=3$ version in the remainder of this paper. Figure 4 shows the same data (as well as some lower-frequency data to be discussed in the next section) plotted in the more conventional way versus $\log_{10}\Omega$. The fit of $F_3(\Omega)\simeq F_3(\omega/2B_\psi\kappa^2)$ to the data that is shown in Figs. 3 and 4 has been obtained by choosing $B_\psi\cong 1.3\times 10^{-4}$ cm^2/sec (the exact value of the kinetic coefficient used for each frequency is given in Fig. 7) and by using

$$\kappa=\kappa_0 t^{2/3} , \quad (2.29)$$

where $\kappa_0=0.70\times 10^8$ cm^{-1} and $t=(T-T_\lambda)/T_\lambda$ is the

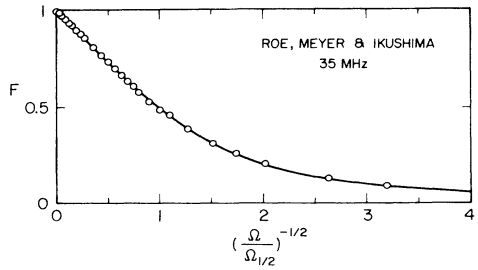

FIG. 3. Three-dimensional attenuation function F vs $\Omega^{-1/2}$, the inverse square root of the scaled frequency. $\Omega=\Omega_{1/2}$ when $F=\frac{1}{2}$. The data points show the 35-MHz attenuation measurements of Ref. 9. The linear drop away from the λ point (at $\Omega=\infty$) is a characteristic feature of the three-dimensional attenuation function.

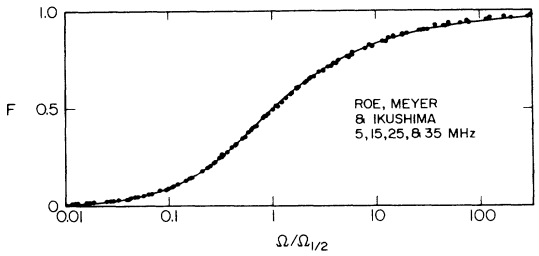

FIG. 4. Attenuation function vs scaled frequency normalized to $\Omega_{1/2}$, its $F=\frac{1}{2}$ value. The data points show the attenuation measurements of Ref. 9 for four different frequencies.

reduced temperature.

In preparing Figs. 3 and 4 it has also been necessary to take into account the denominator in Eq. (2.13). In order to extract experimental numbers for F from the α/α_λ measurements, the attenuation divided by its λ-point value, to compare with the theoretical curve for $F(\Omega)$, it is necessary to cancel out the denominator in Eq. (2.13) by multiplying by

$$|C_p|^2=(\mathrm{Re}C_p)^2+(\mathrm{Im}C_p)^2 . \tag{2.30}$$

Figure 5 shows both the $\omega=0$ thermodynamic specific heat and $\mathrm{Re}C_P$ computed for $\omega/2\pi=35$ MHz. The latter has been obtained from Eqs. (2.17) and (2.18), after adding the amount of background necessary to make Eq. (2.19) consistent with the $\omega=0$ thermodynamic specific heat. The point in Fig. 5 at which the 35-MHz curve merges with the $\omega=0$ curve is also the point at which the imaginary part of the specific heat becomes negligibly small. Thus it is evident that the variation of the real part over the entire temperature range is rather mild; the "processing" to which we subject the data is, therefore, not a radical effect, which furthermore becomes even less pronounced at frequencies smaller than 35 MHz. The result of the processing is obviously largest at the small reduced frequencies, causing the tail in F to be smaller than the tail in α/α_λ.

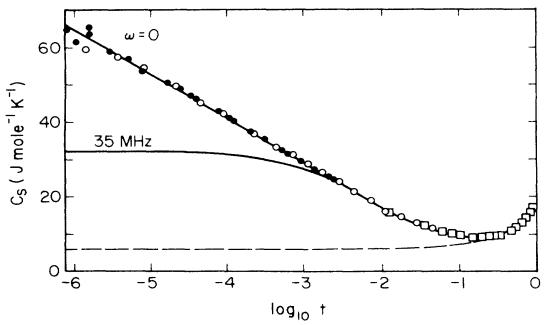

FIG. 5. Specific heat of liquid ^{4}He in J/mol K at saturated vapor pressure vs logarithm of reduced temperature. The data points and the upper curve are reproduced from Fig. 4 of Ref. 5 and show the critical variation of the specific heat in the thermodynamic limit ($\omega=0$). The dashed curve shows the underlying noncritical background. The lower solid curve exhibits the real part of the finite-frequency generalization, which has a nondiverging behavior as the λ point is approached ($t\to 0$).

III. CROSSOVER FREQUENCY REGION

In this section we investigate empirically the effect of lowering the frequency at which the critical ultrasonic attenuation is measured. Our goal is to test a theoretical expectation that is developed in detail in a paper to follow.[7] We find there, to a good approximation, that, in spite of the critical variation of D_ψ which results from going outside the van Hove region, the scaling shape of the attenuation function remains largely unchanged. For the present purposes we can summarize the theoretical prediction as follows: The effect of entering the crossover region can be almost entirely absorbed by an increase in the magnitude of D_ψ, which is treated as an effective adjustable noncritical background kinetic coefficient, B_ψ.

In the preceding section, in order to reveal in as unencumbered a fashion as possible the simple basic features of the theory, we have "processed" the experimental data for α/α_λ, by multiplying by $|C_P|^2$. In this way we can concentrate our attention entirely on $\mathrm{Im}C_P$ without having to contend with the added complication arising from the variation of $\mathrm{Re}C_P$. From a theoretical point of view, the imaginary part of C_P is a more interesting function than its real part. In the van Hove region, at least, $\mathrm{Im}C_P$ is a function of only the one scaled variable Ω, while $\mathrm{Re}C_P$ is necessarily a function of both the temperature and frequency variables, i.e., κ and Z. Furthermore, as discussed and elaborated in detail in Sec. V of Ref. 6, $\mathrm{Re}C_P$ can be obtained from $\mathrm{Im}C_P$ by means of the Kramers-Kronig relation, or, alternatively, the Cauchy-Riemann method. Thus, from a theoretical standpoint, the determination of $\mathrm{Im}C_P$ solves the critical ultrasonic attenuation problem completely. Viewed in this way, the fact that the experimentalists necessarily measure $-\mathrm{Im}C_P^{-1}=\mathrm{Im}C_P/|C_P|^2$ instead of $\mathrm{Im}C_P$ directly has to be regarded as nothing more than an inconvenience that we are forced to deal with in one way or another. Our interest is focused upon Im C_P, rather than upon $-\mathrm{Im}C_P^{-1}$.

It would be quite convenient if the experimentalists could measure the ultrasonic attenuation over a wide range of frequency for every given temperature. The Kramers-Kronig relations would then yield $\mathrm{Re}C_P^{-1}$ from the measurements of $\mathrm{Im}C_P^{-1}$, thereby determining the full complex function C_P^{-1}, and in turn, C_P itself. In the absence of such a desirable state of affairs, we can only bring α/α_λ and $F_3(\Omega)$ together for comparison either by (A) multiplying the former or (B) dividing the latter by $|C_P|^2$. Method A has been used in Figs. 3 and 4. In these figures we compared the "processed" 35-MHz data with the plot of $F_3(\Omega)$ versus $\Omega^{-1/2}$ and $\log_{10}\Omega$, respectively. The more conventional alternative, method B, is shown in Fig. 6. The excellent agreement found between theory and experiment is, of course, independent of which method is employed for the comparison. The difference between the curves of Figs. 4 and 6 sets in at the low-frequency, low-attenuation end, because of the decrease in

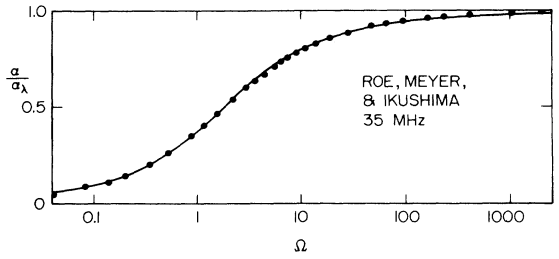

FIG. 6. Comparison of the theory with measurements (Ref. 9) of the dependence of the attenuation on the scaled frequency. The kinetic coefficient has been fixed at $B_\psi = 1.28 \times 10^{-4}$ cm^2/sec.

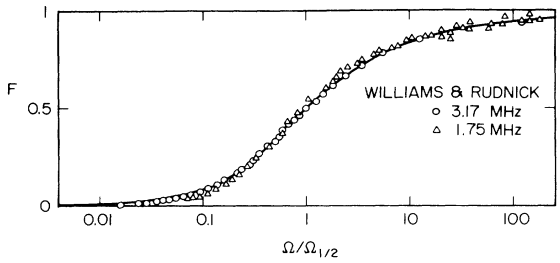

FIG. 8. Attenuation function vs scaled frequency normalized to $\Omega_{1/2}$. The circles and triangles show the measurements of Ref. 11 for 3.17 and 1.75 MHz, respectively.

$|C_P|^2$ as T is raised above T_λ. This difference is already presaged by the shift in the midpoint of Fig. 6. The 50% drop in α/α_λ comes at a value of Ω somewhat smaller than the midpoint value $\Omega_{1/2} = 2.8$ for $F_3(\Omega)$. Comparing the tails of the curves at, say, $\Omega = 0.09$, or one and one-half decades below $\Omega_{1/2}$, we see that the value of α/α_λ is approximately 2.5 times that of F_3. Thus, the percentage difference becomes substantial only in a region where both functions are small.

Because methods A and B are entirely equivalent in terms of testing the theory against the experimental data, we will use mainly method A in the rest of this paper. It has the advantage of permitting the display of runs at different frequencies on the same graph. This is evident in Fig. 4 where we have added the data[9] for the runs at the lower frequencies of 5, 15, and 25 MHz to those at 35 MHz. (The 0.7% admixture of ^{3}He was determined to have less than a 1% effect on α/α_λ.) The resulting agreement with scaling is such that we have made no effort in the figure to identify separately the data points for the different runs. The values of $D_\psi = B_\psi$ required for this scaling are plotted in Fig. 7 as $\nu^{-1/2}$ for the four different values of ν (frequency in MHz).

In our earlier publication[3] we exhibited clear evidence of scaling in the measurements of Tozaki and Ikushima[10] which covered the frequency range 10–163 MHz. The five different runs at 10, 18, 54, 90, and 163 MHz all collapsed onto a single curve. Furthermore, this curve was in satisfactory accord with the theoretically predicted, lowest-order ϵ-expansion curve, i.e., F_4 in the present notation. There was, however, in Fig. 2 of Ref. 3, some indication that the measurements dropped more rapidly from the λ point than F_4. This feature, as well as the collapse of several different runs onto a single curve, is even more clearly evident in the data of Roe *et al.*,[9] as exhibited in Fig. 4 above. It is further apparent that the high-frequency defect in F_4 is remedied by F_3, which takes into account some of the effects of interaction of the fluctuations.

Proceeding to yet lower frequencies, the measurements of Williams and Rudnick[11] at 3.17 and 1.75 MHz take us even further out of the van Hove region and into the crossover region. Figure 8 shows that, here again, $F_3(\Omega)$ gives a good fit to the processed data. The values of $D_\psi = B_\psi$ required for these fits are exhibited by the solid

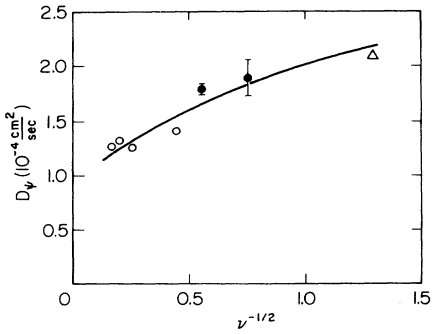

FIG. 7. Kinetic coefficient vs inverse square root of the frequency (in MHz). D_ψ is the effective value of B_ψ, the van Hove parameter. The curve shows the monotonic rise that is expected theoretically when the frequency drops below the van Hove range and enters the precritical crossover region.

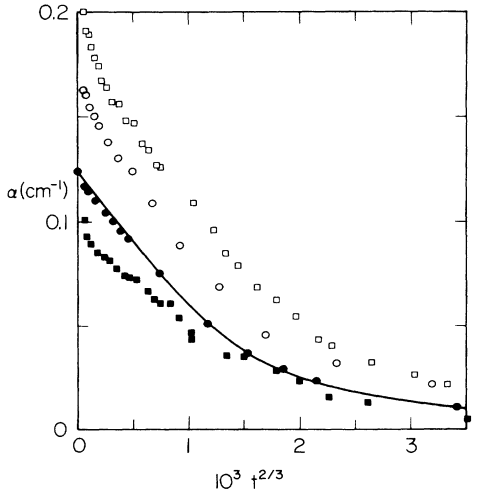

FIG. 9. Attenuation in neper/cm vs $10^3 t^{2/3}$, where t is the reduced temperature, for the two frequencies 1.0 and 0.6 MHz. Data: □, 1 MHz (Ref. 11); ■, 0.6 MHz (Ref. 11); ○, 1 MHz (Ref. 12); ●, 0.6 MHz (Ref. 13). The curve is the two-parameter fit of the theory to the data of Ref. 13, obtained for $\alpha_\lambda = 0.124$ cm^{-1} and $B_\psi = 2.1 \times 10^{-4}$ cm^2/sec, and shows the characteristic linear dependence on $\Omega^{-1/2} \propto t^{2/3}$ near the λ point.

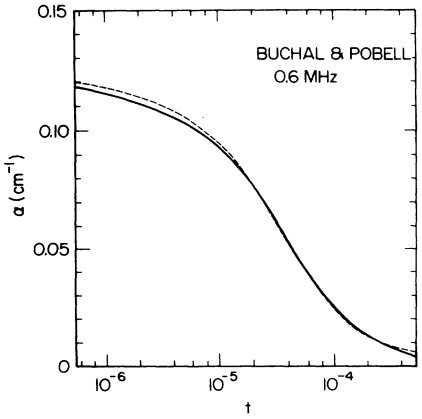

FIG. 10. Comparison of theory (dashed curve) with measurements (Ref. 13) (solid curve) of the temperature dependence of the attenuation at 0.6 MHz. The temperature dependence of α shown by the dashed curve is identical to that shown by the solid curve in Fig. 9.

circles in Fig. 7. The error bars attached to these two entries are intended as a semiquantitative indication of the scatter evident in the data.[11]

Proceeding to even lower frequencies, we are confronted with some discrepancies between the measurements at the same frequencies of Williams and Rudnick[11] on the one hand, and those of Carey, Buchal, and Pobell,[12] and of Buchal and Pobell,[13] on the other hand. These discrepancies are exhibited in Fig. 9. The squares show the Williams-Rudnick[11] values of α in nepers/cm plotted versus $t^{2/3}$. The Carey *et al.*[12] data and the Buchal and Pobell[13] data are displayed by the circles. The open and solid symbols show the measurements at 1.0 and 0.6 MHz, respectively. Neither of the 1.0-MHz runs[14] can be fit by our theory. However, for the 0.6-MHz run of Buchal and Pobell,[13] we find the good fit that is exhibited in Figs. 9 and 10. The solid curve in Fig. 10, which is the same as that of Fig. 9 of Ref. 13, displays the 0.6-MHz measurements of Buchal and Pobell.[13] The solid circles that we have placed on our Fig. 9 were obtained by reading off the curve in Fig. 9 of Ref. 13. The dashed curve in our Fig. 10 shows the same two-parameter theoretical fit as in Fig. 9. As $t^{2/3}$ is, by definition, identical to $\Omega^{-1/2}$ up to a numerical factor, the theoretical curve in Fig. 9 is the same as that shown in Fig. 3, except for the inclusion of the $|C_P|^2$ denominator (method B). A 2% deviation of the theoretical function from the data occurs relatively close to the λ point, at the reduced temperature of $t \simeq 2\times 10^{-6}$, or at the van Hove reduced frequency of $\Omega \simeq 70$.

The value of the kinetic coefficient, $D_\psi = B_\psi = 2.1\times 10^{-4}$ cm^2/sec, that has been used for the fit in Figs. 9 and 10 is exhibited by the triangle in Fig. 7. The monotonic trend of increasing D_ψ with decreasing ν is qualitatively what is to be expected upon leaving the van Hove region and entering the precritical and crossover region.[15–17] The curve in Fig. 7 exhibits the frequency dependence of D_ψ that is indicated by including in the theory dynamic interaction effects to two-loop order.[7] (The absolute strength of the kinetic coefficient has been multiplied by a renormalizing constant so as to bring our predicted curve[7] into agreement with the points in Fig. 7.)

IV. SUMMARY

Guided by some studies of the related problem of the critical attenuation in a binary liquid, we have presented an improved treatment of the same phenomenon in liquid ^{4}He. We have taken the interaction of the order-parameter fluctuations into account to first order by representing the frequency-dependent specific heat by the logarithm of the single-loop integral, computed in three dimensions. As demonstrated in Sec. II, this is clearly an improvement over our earlier $D=4$ theory, which neglected the interactions. As evident in Figs. 3 and 4, the resulting agreement with the experimental data is excellent, both in regard to the scaling property and in regard to the actual fit of F_3, the theoretical three-dimensional (3D) scaling function, to the data. The linear dependence of F_3 on $\Omega^{-1/2}$ that is shown in Fig. 3 is an important characteristic of the 3D theory, and is evidently verified by the data. (This linear dependence on κ near the critical point is, in fact, a general feature of three-dimensional critical dynamics.[18])

In Sec. III we have examined data at frequencies low enough that the order-parameter relaxation rate is no longer expressed by the van Hove formula $B_\psi\kappa^2$. Nevertheless, motivated by our two-loop dynamic calculations, to be presented in a separate paper,[7] we have proceeded here purely phenomenologically, using the single-loop theory. We have found, as demonstrated in Figs. 4, 8, and 10, that the shape of the attenuation function is well fit for frequencies as low as 5, 3.17, 1.75, and even 0.6 MHz. (At and below 1 MHz there is some disagreement in the experimental literature.[11–13]) For each frequency, it is necessary only to multiply B_ψ by a temperature-independent factor. The frequency dependence of this factor is exhibited in Fig. 7 and is in good accord with the theoretical expectation.[7]

ACKNOWLEDGMENTS

We are indebted to Professor Horst Meyer for some helpful discussions. This research has been supported by the U.S. National Science Foundation via Grants for Basic Research DMR 85-06009 and DMR 82-05356.

[1]R. A. Ferrell and J. K. Bhattacharjee, Phys. Lett. **86A**, 109 (1981).
[2]K. E. Herzfeld and F. O. Rice, Phys. Rev. **31**, 691 (1928).
[3]R. A. Ferrell and J. K. Bhattacharjee, Phys. Rev. Lett. **44**, 403 (1980).
[4]E. A. Clerke, J. V. Sengers, R. A. Ferrell, and J. K. Bhattacharjee, Phys. Rev. A **27**, 2140 (1983).
[5]R. A. Ferrell and J. K. Bhattacharjee, Phys. Rev. B **25**, 3168

(1982).
[6]R. A. Ferrell and J. K. Bhattacharjee, Phys. Rev. A **31**, 1788 (1985).
[7]R. A. Ferrell, B. Mirhashem, and J. K. Bhattacharjee (unpublished).
[8]R. A. Ferrell and J. K. Bhattacharjee, Phys. Rev. B **23**, 2434 (1981).
[9]D. B. Roe, H. Meyer, and A. Ikushima, J. Low Temp. Phys. **32**, 67 (1978). We are indebted to Professor Horst Meyer for communication of this data in numerical form.
[10]K. Tozaki and A. Ikushima, J. Low Temp. Phys. **32**, 379 (1978).
[11]D. Williams and I. Rudnick, Phys. Rev. Lett. **25**, 276 (1970).
[12]R. Carey, Ch. Buchal, and F. Pobell, Phys. Rev. B **16**, 3133 (1977).
[13]Ch. Buchal and F. Pobell, Phys. Rev. A **14**, 1103 (1976).
[14]The discrepancy between the 1-MHz measurements of Refs. 11 and 12 is smaller in the normalized attenuation, α/α_λ, which, according to Pankert and Dohm, is in agreement with their computations. [J. Pankert, Ph.D. dissertation, Technische Hochschule Aachen, 1986; J. Pankert and V. Dohm, Europhys. Lett. **2**, 775 (1986).]
[15]R. A. Ferrell and J. K. Bhattacharjee, Phys. Rev. Lett. **42**, 1638 (1979).
[16]J. K. Bhattacharjee and R. A. Ferrell, Phys. Rev. B **25**, 216 (1982).
[17]R. A. Ferrell and J. K. Bhattacharjee, Phys. Rev. B **28**, 121 (1983).
[18]R. A. Ferrell and J. K. Bhattacharjee, J. Stat. Phys. **41**, 899 (1985).